Determining the Maximum Power Transfer Points for MC-WPT Systems With Arbitrary Number of Coils

Yue Sun, *Member, IEEE*, Zhi-Juan Liao, Zhao-Hong Ye, Chun-sen Tang, *Member, IEEE*, and Pei-Yue Wang

***Abstract*—To reveal the general characteristic of the maximum power transfer points of magnetic coupling wireless power transfer (MC-WPT) systems, and to quickly and accurately determine all possible maximum power transfer points for arbitrary coil MC-WPT systems, a novel theoretical analysis method is proposed in this paper. Based on the modal theory, an accurate time-domain model of an *n*-coil MC-WPT system is established and the analytical current response on each coil is derived. According to the current response of the load, a detailed power spectrum distribution is presented, based on which the mathematic expressions of all possible maximum power transfer points, including the maximum output powers and corresponding operating frequencies, are deduced. The theoretical results are verified in experiment prototypes practically. The experimental results show that: 1) the output power reaches its maximum value at the modal frequencies rather than the designed natural frequency of the resonators in MC-WPT systems; 2) there are *n* modal frequencies of an *n*-coil MC-WPT system. The analysis results provide useful information to choose the operating frequency for practical MC-WPT systems with arbitrary number of coils.**

***Index Terms*—Modal frequencies, modal theory, the maximum power transfer, wireless power transfer.**

I. Introduction

MAGNETIC coupling wireless power transfer (MC-WPT) is a technology to transfer power from power sources to electric loads across some large air gaps by electromagnetic coupling. This technology has been a research hotspot since the inspiring work of transmitting 60 W power to a lamp over a distance of 2 m was demonstrated in 2007 [1], [2]. Due to the electric isolation between transmitters and receivers, this technology has the advantages of flexibility, reliability, and safety. In recent years, considerable process in MC-WPT has paved the

Manuscript received September 3, 2017; revised December 16, 2017; accepted January 17, 2018. Date of publication January 30, 2018; date of current version August 7, 2018. This work was supported in part by the National High Technology Research and Development Program of China (863 Program) under Grant 2015AA016201 and in part by the National Natural Science Foundation of China under Grant 61573074. Recommended for publication by Associate Editor D. Qiu. (*Corresponding author: Yue Sun*.)

Y. Sun is with the State Key Laboratory of Power Transmission Equipment & System Security and New Technology, and the College of Automation, Chongqing University, Chongqing 400044, China (e-mail:

For the maximum power points analysis of MC-WPT systems, circuit theory [26]–[28] and coupled mode theory [18], [29] are the two traditional and major analysis methods. In [21], Lee *et al.* investigated the effects of cross couplings of nonadjacent resonators on the optimal frequency for multicoil MC-WPT systems, but this paper did not consider the frequency deviation caused by frequency splitting which could occur even if the cross couplings are negligible. More importantly, the physical interpretation of the optimal frequency is not involved in [21]. Establishing a generalized mathematic relationship between the maximum power transfer points and the electric parameters not only permits quantitative analysis of the optimal frequency but also provides a generic platform for its physical interpretation. In [18], [27]–[29], the analytical frequencies of the maximum power transfer points were derived by using the two traditional methods, but they limited their study to some specific low-order systems with a symmetrical parameter structure and negligible cross couplings. Theoretical investigations of the maximum power transfer points of a nonsymmetrical MC-WPT system were discussed in [26], but the model is the simplest two-coil system. Since the circuit theory and coupled mode theory can only derive the analytical frequencies of the maximum power transfer points by seeking the extreme points of the output power versus the operating frequency, hence the two methods only suit for such specific simple systems. For a multicoil system with nonsymmetrical parameters and nonnegligible cross couplings, the equations would become extremely complex and rigorous to be analyzed with two traditional methods. Actually, an MC-WPT system may have multiple maximum power transfer points, the number and position of which will vary with parameters of the system [30]. So far, the generalized characteristic of the maximum power transfer points of MC-WPT systems is not clear, which has become a bottleneck problem of WPT systems and has practical significance [31], [32].

In this paper, a novel theoretical analysis method in terms of modal theory is proposed for MC-WPT systems with arbitrary number of coils to quickly and accurately determine its maximum power transfer points. With the proposed method, the mathematic expressions of all possible maximum power transfer points of arbitrary coil MC-WPT systems, including the operating frequencies and corresponding output powers, are derived, based on which the generalized characteristic and physical interpretation of the maximum power transfer points are deduced. From engineers' point of view, knowledge of the maximum power transfer points provides useful information for the choice of operation frequency and parameter optimum design for practical use.

This paper is organized as follows: an accurate time-domain model of *n*-coil MC-WPT systems is established in Section II. The analytical current response on each coil along with the mathematic expression of output power is derived based on the modal theory in Section III. In Section IV, a detailed spectrum distribution of the output power is presented to determine the maximum power transfer points, based on which all possible maximum power transfer points, including the maximum powers and corresponding frequencies, are deduced. Finally, prototypes have been built and tested to validate the theoretical analysis.

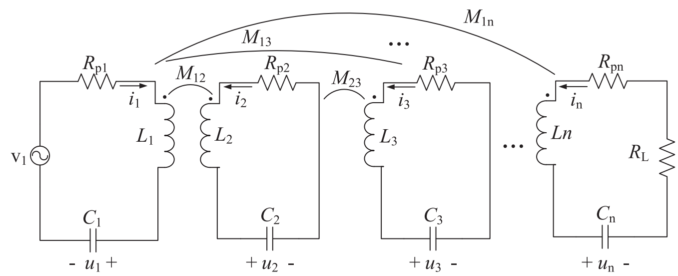

Fig. 1. Equivalent circuit diagram of an *n*-coil MC-WPT system.

II. Mathematic Model of an *N*-Coil MC-WPT System

Fig. 1 shows the equivalent circuit diagram of a typical *n*-coil MC-WPT system. The schematic consists of *n* coils and each coil is connected with a lumped compensating capacitor to form a resonator.

In Fig. 1, variables with the subscript *j* represents the electric parameters in the *j*th resonator ($j = 1,2,\ldots,n$). Rp_j, L_j, and C_j indicate the equivalent series resistance (ESR), self-inductance, and the corresponding compensating capacitor of the *j*th coil, respectively. i_j is the current in the *j*th resonator and u_j is the voltage across capacitor C_j. M_{ij} denotes the mutual inductance between the *i*th coil and *j*th coil ($i \neq j$ and $M_{ij} = M_{ji}$). v_1 and R_L stand for the supply voltage and load resistance of the system, respectively. R_j is defined as the total resistance of the *j*th resonator. When $j \neq n$, $R_j = R_{pj}$, otherwise $R_j = R_{pj} + R_L$.

For mathematical modeling, sinusoidal supply voltage with angular frequency ω is assumed, that is, $v_1 = V\sin(\omega t)$, where *V* is the amplitude of the supply voltage. Then, the natural frequency (ω_{cj}) and quality factor (Q_j) of the *j*th resonator can be obtained as $\omega_{cj} = 1/\sqrt{L_j C_j}$ and $Q_j = \omega L_j / R_j$, respectively. Usually, in order to increase the coupling strengths, the quality factors of the resonators in MC-WPT systems are relatively high [1], [2], [10].

According to Kirchhoff's voltages law (KVL), the mathematic model of the *n*-coil MC-WPT system can be expressed as

$$\begin{cases} L_1 C_1 \ddot{u}_1 + M_{12} C_2 \ddot{u}_2 + \cdots M_{1n} C_n \ddot{u}_n + R_1 C_1 \dot{u}_1 + u_1 = v_1 \\ M_{12} C_1 \ddot{u}_1 + L_2 C_2 \ddot{u}_2 + \cdots M_{2n} C_n \ddot{u}_n + R_2 C_2 \dot{u}_2 + u_2 = 0 \\ \vdots \\ M_{1n} C_1 \ddot{u}_1 + M_{2n} C_2 \ddot{u}_2 + \cdots L_n C_n \ddot{u}_n + R_n C_n \dot{u}_n + u_n = 0. \end{cases} \tag{1}$$

Define $\mathbf{V} = [v_1 \ 0 \cdots 0]^T$, $\mathbf{I} = [i_1 \ i_2 \cdots i_n]^T$, and $\mathbf{U} = [u_1 \ u_2 \cdots u_n]^T$ as the supply voltage vector, current vector, and the capacitor voltage vector of the system, respectively, the mathematic model in (1) can be transformed into

$$\mathbf{LC\ddot{U}} + \mathbf{RC\dot{U}} + \mathbf{U} = \mathbf{V} \tag{2}$$

where

$$\mathbf{L} = \begin{bmatrix} L_1 & M_{12} & \cdots & M_{1n} \\ M_{21} & L_2 & \cdots & M_{2n} \\ \vdots & \vdots & \ddots & \vdots \\ M_{n1} & M_{n2} & \cdots & L_n \end{bmatrix}$$
$$\mathbf{C} = \mathrm{diag}\left(C_1 \ C_2 \ \cdots \ C_n \right)_{n\times n}$$
$$\mathbf{R} = \mathrm{diag}\left(\mathrm{R}_1 \ R_2 \ \cdots \ R_n \right)_{n\times n}. \tag{3}$$

Here, operator $\mathrm{diag}(\cdot)_{n\times n}$ represents the generation of an n-order diagonal matrix, i.e.,

$$\mathrm{diag}\left(a_1 \ a_2 \ \cdots \ a_n \right)_{n\times n} = \begin{bmatrix} a_1 & 0 & \cdots & 0 \\ 0 & a_2 & \cdots & 0 \\ \vdots & \vdots & \ddots & \vdots \\ 0 & 0 & \cdots & a_n \end{bmatrix}. \tag{4}$$

III. System Response Analysis With Modal Theory

Modal analysis is often used to analyze and optimize dynamic characteristics of mechanic vibration systems, which is the process of determining the inherent dynamic characteristics of a system in terms of its modal parameters, including modal frequencies, damping coefficients, and mode shapes. This method is based upon the fact that the response of a linear time-variant dynamic system with a mathematic model in the form as shown in (2) can be expressed as the linear combination of a set of simple harmonic waves called modes [33]. In this paper, the current response on each coil will be derived with modal theory, and then, the power spectrum distribution of the system will be deeply investigated to determine the maximum power transfer points.

According to the matrix theory, there is a nonsingular matrix $\mathbf{\Phi} = [\{\boldsymbol{\varphi}\}_1, \{\boldsymbol{\varphi}\}_2, \cdots \{\boldsymbol{\varphi}\}_n]_{n\times n}$, which makes (5) established [34]. The qth column vector $\{\boldsymbol{\varphi}\}_q = [\, \varphi_{1q} \ \varphi_{2q} \ \cdots \ \varphi_{nq} \,]^{\mathrm{T}}$ in matrix $\mathbf{\Phi}$ is called qth mode shape of the system. It should be noticed that, different from the subscript j in Fig. 1 which denotes the circuit elements in the jth resonator, here the subscript q emphasizes the position of the column $\{\boldsymbol{\varphi}\}_q$ in matrix $\mathbf{\Phi}$

$$\begin{cases} \mathbf{\Phi}^T \mathbf{L}\mathbf{C}\mathbf{\Phi} = \tilde{\mathbf{M}} = \mathrm{diag}(\, m_1 \ m_2 \ \cdots \ m_n \,)_{n\times n} \\ \mathbf{\Phi}^T \mathbf{\Phi} = \tilde{\mathbf{K}} = \mathrm{diag}(\, k_1 \ k_2 \ \cdots \ k_n \,)_{n\times n} \end{cases} \tag{5}$$

where $m_q = \{\boldsymbol{\varphi}\}_q^T (\mathbf{LC}) \{\boldsymbol{\varphi}\}_q$, $k_q = \{\boldsymbol{\varphi}\}_q^T \{\boldsymbol{\varphi}\}_q$, and $q = 1, 2, \ldots, n$.

Unlike the usual approach used for linear vibration systems, in which one computes the natural modes in general by using complex matrix calculus, here we use real matrix calculus by assuming that the matrix $\mathbf{\Phi}^T \mathbf{RC\Phi}$ is a diagonal matrix, that is, the nondiagonal elements in matrix $\mathbf{\Phi}^T \mathbf{RC\Phi}$ are assumed to be zero, i.e., $\mathbf{\Phi}^T \mathbf{RC\Phi} \approx \tilde{\mathbf{C}} = \mathrm{diag}(\, c_1 \ c_2 \ \cdots \ c_n \,)_{n\times n}$, where $c_q = \{\boldsymbol{\varphi}\}_q^T (\mathbf{RC}) \{\boldsymbol{\varphi}\}_q$. The effects of this assumption can be ignored when the damping coefficients of the system are small [33]. For MC-WPT systems, due to the generally high quality factor of resonators, the damping coefficients are usually very small and then the assumption is justified, which will be demonstrated later. In this case, the mathematic model of the system shown in (2) can be decoupled into n mutual independent equations as follows:

$$\tilde{\mathbf{M}}\ddot{\mathbf{X}} + \tilde{\mathbf{C}}\dot{\mathbf{X}} + \tilde{\mathbf{K}}\mathbf{X} = \mathbf{Y} \tag{6}$$

where

$$\mathbf{X} = \mathbf{\Phi}^{-1}\mathbf{U} = \begin{bmatrix} x_1 \\ x_2 \\ \vdots \\ x_n \end{bmatrix}, \ \mathbf{Y} = \mathbf{\Phi}^T \mathbf{V} = \begin{bmatrix} y_1 \\ y_2 \\ \vdots \\ y_n \end{bmatrix}. \tag{7}$$

Substituting $\mathbf{V} = [\, v_1 \ 0 \cdots \ 0 \,]^T$ and $v_1 = V\sin(\omega t)$ into (7), the qth element in vector $\mathbf{Y}$ can be obtained as $y_q = \{\boldsymbol{\varphi}\}_q^T \mathbf{V} = \varphi_{1q} V \sin(\omega t)$. In this case, the qth independent equation in (6) can be expressed as

$$m_q \ddot{x}_q + c_q \dot{x}_q + k_q x_q = \varphi_{1q} V \sin(\omega t). \tag{8}$$

Solving for (8), x_q can be derived as

$$x_q = A_{x_q} \sin\left(\omega t + \theta_{x_q}\right) \tag{9}$$

where

$$A_{x_q} = \frac{\varphi_{1q} V}{\sqrt{\left(k_q - m_q\omega^2\right)^2 + c_q^2\omega^2}}$$
$$\theta_{x_q} = \tan^{-1}\left(\frac{-c_q\omega}{k_q - m_q\omega^2}\right). \tag{10}$$

Substituting (9) into

$$\mathbf{U} = [\{\boldsymbol{\varphi}\}_1, \{\boldsymbol{\varphi}\}_2, \cdots \{\boldsymbol{\varphi}\}_n] \begin{bmatrix} x_1 \\ x_2 \\ \vdots \\ x_n \end{bmatrix}$$

and $\mathbf{I} = \mathbf{C}[\, \frac{du_1}{dt} \ \frac{du_2}{dt} \ \cdots \ \frac{du_n}{dt} \,]^T$, the analytical expression of the current vector can be obtained as

$$\mathbf{I} = \mathbf{C}\left(\sum_{q=1}^{n}\left(\{\boldsymbol{\varphi}\}_{\mathbf{q}} \omega A_{xq} \cos\left(\omega t + \theta_{x_q}\right)\right)\right). \tag{11}$$

Then, the analytical current response on each circuit can be quickly determined. For example, the current response on the jth resonator (i_j) can be expressed as

$$i_j = \sum_{q=1}^{n}\left(C_j \varphi_{jq} \omega A_{xq} \cos\left(\omega t + \theta_{x_q}\right)\right) \tag{12}$$

$$|i_j| = C_j \sqrt{\left(\sum_{q=1}^{n} \frac{\varphi_{1q}\varphi_{jq}\omega^2 c_q V}{\left(k_q - m_q\omega^2\right)^2 + c_q^2\omega^2}\right)^2 + \left(\sum_{q=1}^{n} \frac{\varphi_{1q}\varphi_{jq}\omega V\left(k_q - m_q\omega^2\right)}{\left(k_q - m_q\omega^2\right)^2 + c_q^2\omega^2}\right)^2}. \tag{13}$$

which is a linear combination of *n* harmonic waves with amplitude $C_j \varphi_{jq} \omega A_{xq}$. Thus, the amplitude of the current i_j as shown in (12) can be calculated by equation(13) as shown at the bottom of the previous page

From (13) the output power (*P*) and the transfer efficiency (η) of the system can be derived as

$$\begin{aligned} P &= |i_n|^2 R_L/2 \\ &= \frac{R_L C_n^2}{2} \left[\left(\sum_{q=1}^{n} \frac{\varphi_{1q}\varphi_{nq}\omega^2 c_q V}{(k_q - m_q\omega^2)^2 + c_q^2\omega^2} \right)^2 \right. \\ &\quad \left. + \left(\sum_{q=1}^{n} \frac{\varphi_{1q}\varphi_{nq}\omega V \left(k_q - m_q\omega^2\right)}{(k_q - m_q\omega^2)^2 + c_q^2\omega^2} \right)^2 \right] \end{aligned} \tag{14}$$

$$\eta = \frac{|i_n|^2 R_{Ln}}{\sum_{j=1}^{n} |i_j|^2 (R_{pj} + R_{Lj})}. \tag{15}$$

IV. Predication of the Maximum Power Transfer Points

A. Multiple Maximum Power Transfer Points

Since the load resistance R_L is independent of operating frequency ω, according to (14) we can obtain that the frequencies of the maximum power transfer points are equivalent to the frequencies of the maximum current amplitude points of $|i_n|$. Then, the spectrum distribution of current amplitude $|i_n|$ will be deeply investigated in this section to determine the maximum power transfer points.

For simplicity, the current response on the *n*th resonator (i_n) is rewritten as

$$i_n = \sum_{q=1}^{n} \left(C_n \varphi_{nq} B_q \cos\left(\omega t + \theta_{x_q}\right)\right) \tag{16}$$

where

$$B_q = \omega A_{xq} = \frac{\varphi_{1q} V}{\sqrt{m_q k_q}} \frac{1}{\sqrt{\left(\left(\frac{\omega}{\omega_q}\right) - \left(\frac{\omega}{\omega_q}\right)^{-1}\right)^2 + (2\varsigma_q)^2}}. \tag{17}$$

ω_q and ς_q in (17) are defined as the *q*th modal frequency and *q*th damping coefficient of the system, which can be calculated by

$$\omega_q = \sqrt{\frac{k_q}{m_q}}, \varsigma_q = \frac{c_q}{\left(2\sqrt{m_q k_q}\right)}. \tag{18}$$

Then, we can obtain that there are *n* modal frequencies and *n* corresponding damping coefficients of an *n*-coil MC-WPT system. In order to distinguish the modal frequencies of the system from the RNFs ($\omega_{c1}, \omega_{c2}, \ldots, \omega_{cn}$) in the system, the *n* modal frequencies are labeled as $\omega_1, \omega_2, \ldots, \omega_n$. In addition, from (18) we can obtain that the damping coefficients are inversely proportional to the quality factors of the resonators for $c_q = \{\boldsymbol{\varphi}\}_q^T(\mathbf{RC})\{\boldsymbol{\varphi}\}_q$ and $m_q = \{\boldsymbol{\varphi}\}_q^T(\mathbf{LC})\{\boldsymbol{\varphi}\}_q$. Hence, the damping coefficients of MC-WPT systems will be very small as the quality factors of the resonators are relatively high in typical MC-WPT systems.

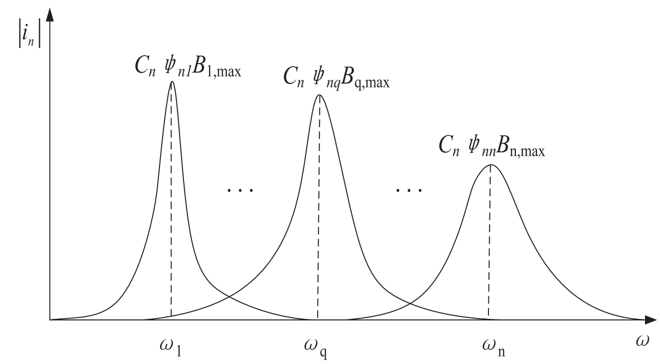

Fig. 2. Spectrum distribution diagram of current amplitude $|i_n|$, which is linearly superimposed by *n* unimodal curves.

B_q versus the operating frequency ω is a unimodal curve and the curve reaches the maximum value $B_{q,\max}$ when ω equals to the *q*th modal frequency ω_q, i.e.,

$$B_{q,\max} = B_q|_{\omega=\omega_q} = \frac{\varphi_{1q} V}{\sqrt{m_q k_q}} \frac{1}{2\varsigma_q}. \tag{19}$$

Since the damping coefficients of MC-WPT systems are usually small, B_q will be much larger than the other items B_s ($q \neq s$) when the operating frequencies ω equals to the *q*th modal frequency ω_q. In this case, the current response i_n can be approximated as $i_n|_{\omega=\omega_q} \approx C_n \varphi_{nq} B_{q,\max} \cos(\omega_q t + \theta_{x_q})$ and $|i_n|$ reaches a local maximum value. Then, the spectrum distribution of the current amplitude $|i_n|$ can be plotted as in Fig. 2.

As shown in Fig. 2, the current amplitude $|i_n|$ is superimposed by *n* unimodal curves with peak positions of $\omega_1, \omega_2, \ldots, \omega_n$. In order to facilitate subsequent analysis, the unimodal curve whose peak position equals to the *q*th modal frequency is labeled as the curve *q*. It is obvious that if the *n* modal frequencies are far away from each other, there are *n* peak positions of the current amplitude $|i_n|$ and the output power, which are equal to the *n* modal frequencies of the system. When some of modal frequencies are very close, there will be a decrease of the peak positions of the superimposed curve (current amplitude $|i_n|$). For example, if the modal frequencies ω_p and ω_q are very close, the superimposed curve composed by the curve *p* and *q* may be changed from the bimodal curve to a new unimodal curve with the peak position in the middle of ω_p and ω_q. But even in this case, the system operating at the natural frequency ω_p or ω_q will also achieve a larger current amplitude because the two modal frequencies ω_p and ω_q are very close to the peak position of the superimposed curve composed by the curve *p* and *q*. The phenomenon of the reduction of the peak positions of the superimposed curve is defined as the mode overlap phenomenon. Theoretically, when some damping coefficients are very large, even if the modal frequencies are not very close, there might be mode overlap phenomenon. But this phenomenon generally does not occur in MC-WPT systems because damping coefficients of MC-WPT systems are general small, that is to say the mode overlap phenomenon of MC-WPT systems occurs only when some modal frequencies are very close.

From the above analysis, we can obtain that only when all modes are overlapping and there is only one peak of current amplitude $|i_n|$, the system is in nonsplitting region, otherwise the system is in splitting region. For MC-WPT systems, since the mode overlap phenomenon occurs only when some modal frequencies are very close, hence the system operating at its modal frequencies will achieve a larger output power no matter whether there is mode overlap phenomenon or not (no matter whether the system is in nonsplitting region or not).

B. Derivation of the Analytical Frequencies of the Maximum Power Transfer Points

The above section has demonstrated that, no matter the system is in splitting or non-splitting state, the system operating at the modal frequencies will achieve a larger output power. However, the derivation of modal frequencies is a bit complicated for practical use. In order to quickly determine the frequencies of the maximum power transfer points, it is necessary to establish a direct mathematic relationship between the modal frequencies and electric parameters

By transforming (3), we have

$$(\mathbf{LC})^{-1}\mathbf{\Phi} = \mathbf{\Phi}\mathbf{M}_p^{-1}\mathbf{K}_p. \tag{20}$$

Then, we can obtain

$$(\mathbf{LC})^{-1}\left[\{\varphi\}_1, \{\varphi\}_2 \cdots \{\varphi\}_n\right] = \left[\{\varphi\}_1, \{\varphi\}_2 \cdots \{\varphi\}_n\right]\begin{bmatrix} \omega_1^2 & 0 & \cdots & 0 \\ 0 & \omega_2^2 & \cdots & 0 \\ \vdots & \vdots & \ddots & \vdots \\ 0 & 0 & \cdots & \omega_n^2 \end{bmatrix}. \tag{21}$$

Equation (21) represents an eigenvalue problem where ω_q^2 is the eigenvalue, $\{\varphi\}_q$ is the corresponding eigenvector of matrix $(\mathbf{LC})^{-1}$, and $q = 1,2,\ldots,n$. Then, the n modal frequencies can be calculated by

$$\omega_{1,\ldots,n} = \sqrt{\text{eigenvalue}\left((\mathbf{LC})^{-1}\right)}. \tag{22}$$

The results indicate that: 1) there are n modal frequencies of an n-coil MC-WPT system, which are the square roots of the eigenvalues of matric $(\mathbf{LC})^{-1}$ and completely determined by the physical properties (L_j, C_j) and spatial distributions (M_{ij}) of the system. 2) All possible frequencies of the maximum power transfer points of arbitrary coil system can be quickly and accurately calculated by using (22).

C. Maximum Output Power Analysis

Since the mode shape $\{\varphi\}_q$ is the corresponding eigenvector of the matrix $(\mathbf{LC})^{-1}$, then $\{\varphi\}_q$, $m_q = \{\varphi\}_q^T(\mathbf{LC})\{\varphi\}_q$, $c_q = \{\varphi\}_q^T(\mathbf{RC})\{\varphi\}_q$, and $k_q = \{\varphi\}_q^T\{\varphi\}_q$ can be quickly determined. Substituting them into (14) and (15) the output power and transfer efficiency of the system at arbitrary operating frequency point can be quickly determined, including the power and efficiency at the modal frequencies.

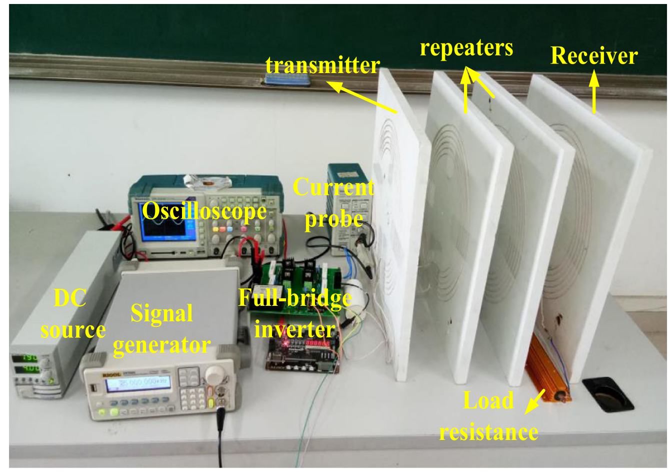

Fig. 3. Photograph of the experimental setup of the four-coil system.

TABLE I
GEOMETRIC PARAMETERS OF THE PRACTICAL COILS

Symbol	Parameters	Values
N	Number of turns	6
a	Inner radius of coil	0.1 m
Wth	Width between per turn	0.01 m
r_wire	Radius of copper wire	0.00125 m

From (14), the output power of the system at the sth modal frequency can be derived as

$$P|_{\omega=;\omega_s} = \frac{R_L C_n^2}{2}\left[\left(\sum_{q=1}^{n}\frac{\varphi_{1q}\varphi_{nq}\omega_s^2 c_q V}{\left(k_q - m_q\omega_s^2\right)^2 + c_q^2\omega_s^2}\right)^2 + \left(\sum_{q=1}^{n}\frac{\varphi_{1q}\varphi_{nq}\omega_s V\left(k_q - m_q\omega_s^2\right)}{\left(k_q - m_q\omega_s^2\right)^2 + c_q^2\omega_s^2}\right)^2\right]. \tag{23}$$

Then, all possible maximum power transfer points, including the frequencies and corresponding output power, can be quickly obtained by using (22) and (23), based on which the optimal frequency of the maximum output power can be quickly determined.

V. Experimental Verification

A. Experimental Setup

In order to validate the theoretical results, several experimental setups have been built and tested (Fig. 3 shows the experimental setup with four coils). All the coils are designed with the same geometric parameters listed in Table I and are aligned centered to the coil centers $r = 0$ along the z-axis. Then, the mutual inductance between two coils is completely determined by the distance of the two coils. The circuit schematic of the experimental setups is shown in Fig. 4. An H-bridge consisting of four MOSFETs is used as the voltage source, which is coupled to the leftmost coil acting as the transmitter. The rightmost coil is the receiver loading by a resistance. The rest of the coils

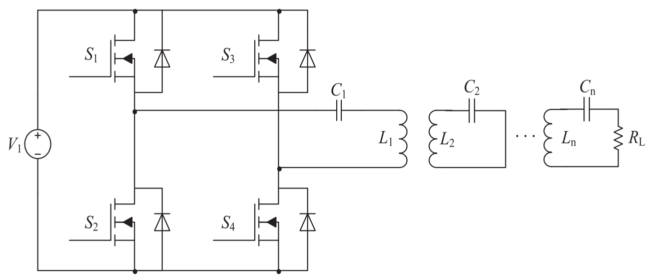

Fig. 4. Circuit schematic of the practical systems.

TABLE II
MUTUAL INDUCTANCES AT DIFFERENT TRANSFER DISTANCES

Transfer distance (m)	0.05	0.1	0.15
Mutual inductance (μH)	5.3	2.55	1.52

TABLE III
GEOMETRIC PARAMETERS OF THE PRACTICAL COILS

System structure	Modal frequencies (kHz)	Output power (W)
The two-coil system	72, 107	26.84, 27.79
The tri-coil system	66, 93, 114	20.06, 27.03, 16.99
The four-coil system	62, 86, 103, 117	16.67, 22.27, 31.3, 10.33

are regarded as repeaters. The measured self-inductance and ESR of the coils are $L_j = 13.8\ \mu$H and $R_{pj} = 0.087\ \Omega$, and the compensating capacitor of each coil is fixed at $259 \pm 10\%$ nF. Then, we can obtain that the natural frequency of each resonator in the practical systems is about 84 kHz.

B. Model Evaluation and the Maximum Power Transfer Points Evaluation

A novel theoretical analysis method for MC-WPT systems is proposed in this paper, based on which the analytical current on each circuit and the mathematic expressions of all possible maximum power transfer points of arbitrary coil MC-WPT systems are derived. In order to verify the proposed theoretical model and testify its accuracy, three experimental setups with two, three, and four coils are demonstrated here. In this set of experiments, the transfer distances between adjacent coils are fixed at 0.05 m and the measured mutual inductances at different transfer distances are listed in Table II. The supply voltage is 7.9 V and the load resistance is 1 Ω (the actually measured value is 0.7 Ω).

Based on the given electric parameters, all possible maximum power transfer points of each system, including the operating frequencies calculated by (22) and corresponding output power calculated by (23), are listed as shown in Table III. Then, the optimal frequency for the maximum power transfer can be quickly and accurately determined, i.e., the optimal frequency of the two-coil system, three-coil system, and four-coils system are 107, 93, and 86 kHz, respectively.

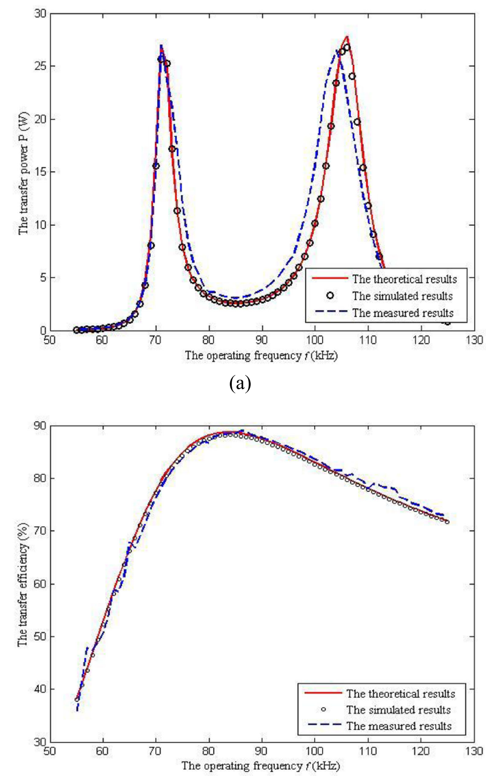

(a)

(b)

Fig. 5. Output power and transfer efficiency versus operating frequency of the two-coil system. (a) Output power. (b) Efficiency.

With the same electric parameters, the systems have been simulated in SIMULINK software. The theoretical, simulated, and measured output power and transfer efficiency versus the operating frequency of the two-coil system, three-coil system, and four-coil system are plotted in Figs 5–7, respectively.

As shown in Figs 5–7, the theoretical output powers and transfer efficiencies at arbitrary operating frequency points are consistent well with the simulated results, which indicate that the proposed theoretical model in this paper is effective and accurate. There are some derivations between the theoretical values and measured values, which mainly caused by the measurement error of electric parameters. In addition, from Figs. 5–7 we can obtain that the extreme points of output power and transfer efficiency are not equal, but the power transfer of each system is relatively efficient at the maximum power transfer points.

Meanwhile, from Figs. 5–7 we can obtain that there are n peak positions of the output power of the n-coil system, which are derived from the designed RNF (84 kHz) and equal to the modal frequencies of the systems as calculated in Table III. The results demonstrate that: 1) the output power reaches its maximum value at the modal frequency points rather than the designed natural frequency point of resonators in MC-WPT systems; 2) there are n modal frequencies of an n-coil MC-WPT system, which can be quickly and accurately determined by using (22).

In order to obtain a better understanding about the power boost ability with the proposed method, the output powers at the optimal frequencies calculated by the proposed method and the

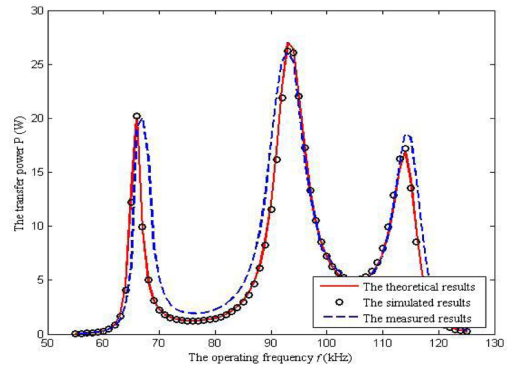

(a)

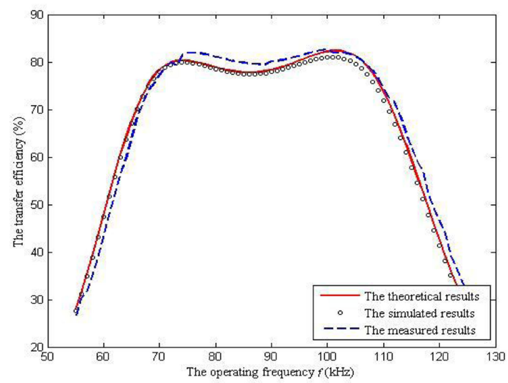

(b)

Fig. 6. Output power and transfer efficiency versus operating frequency of the three-coil system. (a) Output power. (b) Efficiency.

TABLE IV
OUTPUT POWER AT THE OPTIMAL FREQUENCY AND THE DESIGNED RNF

System structure	Power at the modal frequencies (W)	Power at the designed RNF (W)
The two-coil system	27.79	2.567
The tri-coil system	27.03	2.446
The four-coil system	22.17	14.23

designed circuit natural frequency (84 kHz) of the three systems are listed in Table IV. It can be clearly seen from Table IV that the output power has a great improvement by changing the operating frequency from the designed RNF to the optimal frequency calculated by the proposed method.

C. Power Characteristic of Different Mutual Inductances (Transfer Distances)

The theoretical analysis indicates that: 1) the main reason leading to mode overlap phenomenon is the too close distribution of modal frequencies, which will result in a decrease of maximum power transfer points; 2) the system operating at any one of the modal frequencies will achieve a larger power transfer. For verification, the two-coil system is demonstrated in this section.

Since the self-inductances and compensating capacitors of the coils are usually fixed in MC-WPT systems, from (22) we can obtain that the mutual inductances are the main parameters affecting the modal frequencies. A one-to-one relationship between the mutual inductance and the transfer distance is established and inserted into the calculation of the modal frequencies. In this set of experiments, the transfer distance d varies from 0.04 to 0.28 m with a step size of 0.02 m. The predicating frequencies (the theoretical modal frequencies) and the measured frequencies of the maximum power transfer points versus the transfer distance d are plotted in Fig. 8. Fig. 9 shows the

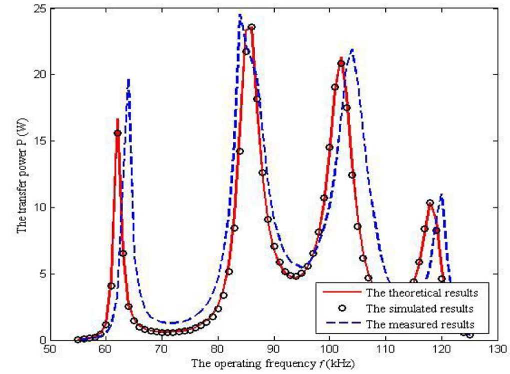

(a)

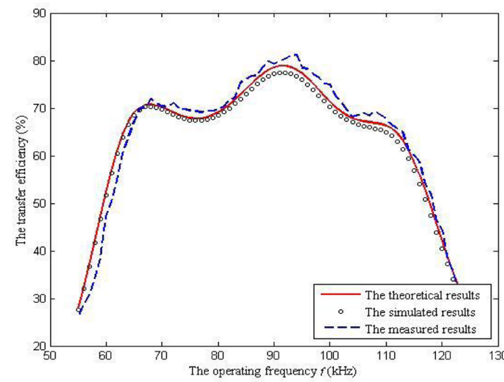

(b)

Fig. 7. Output power and transfer efficiency versus operating frequency of the four-coil system. (a) Output power. (b) Efficiency.

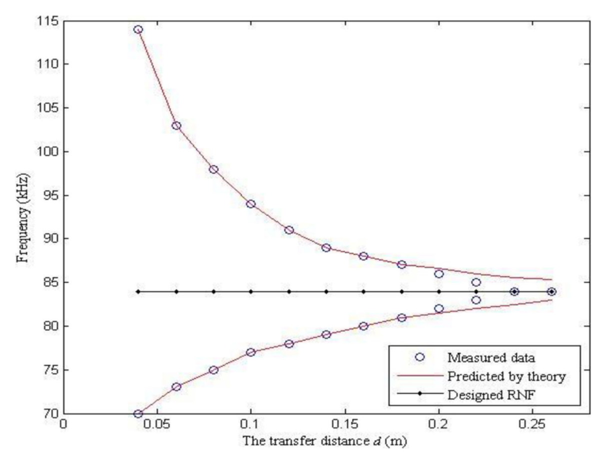

Fig. 8. Frequencies of the maximum power transfer points versus transfer distance d.

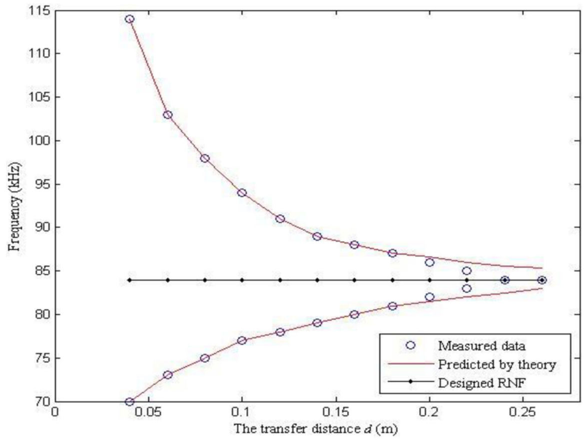

Fig. 9. Measured output power, as a function of transfer distance d, at the first modal frequency and the designed RNF.

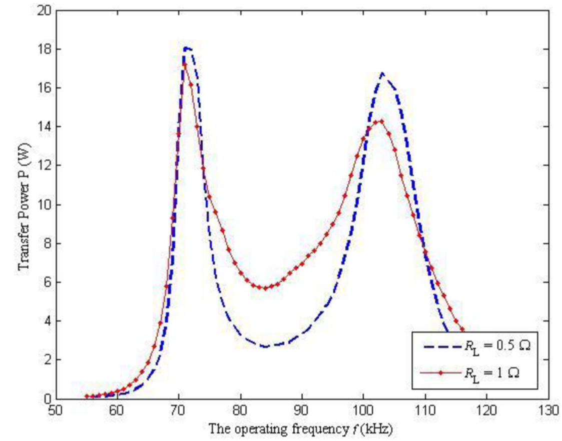

Fig. 10. Measured output power versus the operating frequency at different load resistance.

measured output power versus the transfer distance d when the system operating frequency is set at the first modal frequency (just for comparison, the two modal frequencies can be either one) and the designed RNF.

When the transfer distance is small (the mutual inductance is large), as shown in Figs 8 and 9, the two modal frequencies are far apart and the output power at the modal frequency are extremely larger than that of the designed RNF. The results indicate that the system is in splitting region. In this case, as shown in Fig. 8, the measured frequencies of the maximum power transfer points are consistent well with the theoretical value. With the increase of the transfer distance, as shown in Fig. 8, the frequencies of the maximum power transfer points are getting closer and eventually converge to the designed RNF. Though, in this case, there are some derivations between modal frequency points and maximum power transfer points, the system operating at the modal frequencies also achieves a larger output power as the deviation is very small, which is shown in Fig. 9. Moreover, the derivations will get smaller and smaller with the increase of the transfer distance. Hence, no matter the system is in splitting or nonsplitting region, the system operating at the optimal frequencies will achieve a larger output power.

D. Power Characteristic of Load Resistance

From the above theoretical analysis we can obtain that the load resistance has no relationship with the modal frequencies but has an impact on the damping coefficients. Theoretically, larger damping coefficients may also cause the mode overlap phenomenon and then the decrease of the maximum power transfer points. Since the quality factors of resonators in MC-WPT systems are relatively high and the damping coefficients of MC-WPT systems are very small, the mode overlap phenomenon caused by damping coefficients does not occur in MC-WPT systems in general. The two-coil system in Section V-B is also used here for verification.

Since the operating frequencies of the experiments are about 100 kHz, the self-inductances of the coils are about 13.8 μH, and the ESRs of the coils are about 0.087 Ω, the load resistance should be much less than 0.1 Ω in order to guarantee that the resonators' quality factor is greater than 10 (which usually far larger than 10). In practice, higher operating frequency or coils with larger self-inductance will be chosen for a larger load resistance. For a load resistance of 0.5 and 1 Ω, the measured output power versus the operating frequency is plotted in Fig. 10.

As can been seen from Fig. 10, even though the load resistance is as large as 1 Ω (for general situation, the load resistance in this system should be less than 0.1 Ω), there is no mode overlap phenomenon and the output power peaks at the modal frequencies of the system. The experimental results indicate that the mode overlap phenomenon caused by the load resistance (damping coefficients) does not happen in MC-WPT systems in general and the assumption of small damping coefficients of MC-WPT systems is justified. Although the load resistance has little effect on the frequencies of the maximum power transfer points, as shown in Fig. 10, it has a large effect on the output power.

VI. Conclusion

This paper proposes a novel analysis method for arbitrary coil MC-WPT systems to quickly and accurately determine its maximum power transfer points, including the operating frequencies and corresponding output powers. The method is based on the modal theory and the accurate calculation of the modal frequencies. Contrary to the common sense, it has been theoretically and experimentally demonstrated that:

1) the output power of MC-WPT systems peaks at the modal frequencies of the system rather than the designed natural frequencies of the resonators;
2) no matter the system is in splitting or nonsplitting region, the system operating at the modal frequencies will achieve a larger output power;
3) there are n modal frequencies of an n-coil system, whose mathematic expressions are derived in this paper.

The analysis results provide useful information for the choice of the operating frequency for practical systems. Meanwhile, the theoretical results are also suitable for optimizing the output power by designing the parameters of the system in the future for the accurate relationship between the maximum output power and electric parameters of the system is derived. In addition, since the analytical current on each circuit is derived, then the theoretical method is particularly suitable for analyzing multicoil systems, such as the multitransmitter systems and/or multireceiving systems.

Moreover, since the modal parameters, such as modal frequencies and mode shapes, are inherent to a system and are completely determined by physical properties and spatial distributions of the system, these proposed theoretical results would be possible to be adopted to identify the coupling factors and/or loads of the MC-WPT systems. The multiple modal frequencies characteristic also can be used for designing multiband wireless power transfer systems in the future.

References

[1] A. Karalis, J. D. Joannopoulos and M. Soljačić, "Efficient wireless nonradiative mid-range energy transfer," *Ann. Phys.*, vol. 323, pp. 34–48, Apr. 2008.

[2] A. K. Kurs, R. Moffatt, J. D. Joannopoulos, P. Fisher, and M. Soljacic, "Wireless power transfer via strongly coupled magnetic resonances," *Science*, vol. 317, pp. 83–86, Jul. 2007.

[3] Y. T. Jang and M. M. Jovanovic, "A contactless electrical energy transmission system for portable-telephone battery chargers," *Electronics*, vol. 50, pp. 520–527, Jun. 2003.

[4] A. Sample, B. H. Waters, S. T. Wisdom, and J. R. Smith, "Enabling seamless wireless power delivery in dynamic environments," *Proc. IEEE*, vol. 101, no. 6, pp. 1343–1358, Apr. 2013.

[5] Q. Chen, S. C. Wong, C. K. Tse, and X. Ruan, "Analysis, design, and control of a transcutaneous power regulator for artificial hearts," *IEEE Trans. Biomed. Circuits Syst.*, vol. 3, no. 1, pp. 23–31, Feb. 2009.

[6] C. Yi and B. Xu, "Wireless power transfer for implantable ventricular assistance," *Trans. China Electrotech. Soc.*, vol. 30, pp. 103–109, Mar. 2015

[7] J. Lee and B. Han, "A bidirectional wireless power transfer EV charger using self-resonant PWM," *IEEE Trans. Power Electron.*, vol. 30, no. 4, pp. 1784–1787, Nov. 2015.

[8] Y. S. Hu, Z. Wang, C. Tang, and Q. Xiong, "Design of magnetic coupler for EVs' wireless charging," *Int. J. Appl. Electromagn. Mech.*, vol. 43, pp. 195–205, Oct. 2013.

[9] M. Kung and K. Lin, "Enhanced analysis and design method of dual-band coil module for near-field wireless power transfer systems," *IEEE Trans. Microw. Theory Techn.*, vol. 63, no. 3, pp. 821–832, Mar. 2015.

[10] S. Y. R. Hui, W. Zhong, and C. K. Lee, "A critical review of recent progress in mid-range wireless power transfer," *IEEE Trans. Power Electron.*, vol. 29, no. 9, pp. 4500–4511, Apr. 2014.

[11] W. X. Zhong, C. Zhang, X. Liu, and S. Y. R. Hui, "A methodology for making a three-coil wireless power transfer system more energy efficient than a two-coil counterpart for extended transfer distance," *IEEE Trans. Power Electron.*, vol. 30, no. 2, pp. 933–942, Oct. 2015.

[12] Z. Ye, Y. Sun, X. Dai, C. Tang, Z. Wang, and Y. Su, "Energy efficiency analysis of U-Coil wireless power transfer system," *IEEE Trans. Power Electron.*, vol. 31, no. 7, pp. 4809–4817, Jan. 2016.

[13] Y. Zhang, T. Lu, Z. Zhao, F. He, K. Chen, and L. Yuan, "Selective wireless power transfer to multiple loads using receivers of different resonant frequencies," *IEEE Trans. Power Electron.*, vol. 30, no. 11, pp. 6001–6005, Nov. 2015.

[14] P. Sample, D. A. Meyer, and J. R. Smith, "Analysis, experimental results, and range adaptation of magnetically coupled resonators for wireless power transfer," *IEEE Trans. Ind. Electron.*, vol. 58, no. 2, pp. 544–554, Feb. 2011.

[15] Y. Zhang, Z. Zhao, and K. Chen, "Frequency-splitting analysis of four-coil resonant wireless power transfer," *IEEE Trans. Ind. Appl.*, vol. 50, no. 4, pp. 2436–2445, Jul./Aug. 2014.

[16] D.-W. Seo, J.-H Lee and H.-S. Lee, "Optimal coupling to achieve maximum output power in a WPT system," *IEEE Trans. Power Electron.*, vol. 31, no. 6, pp. 3994–3998, Jun. 2016.

[17] Y. Lim, H. Tang, S. Lim, and J. Park, "An adaptive impedance-matching network based on a novel capacitor matrix for wireless power transfer," *IEEE Trans. Power Electron.*, vol. 29, no. 4, pp. 4403–4413, Mar. 2014.

[18] W. Niu, W. Gu, J. Chu, and A. Shen, "Frequency splitting patterns in wireless power relay transfer," *IET Circuits Devices Syst.*, vol. 8, pp. 561–567, Jul. 2014.

[19] Y. Lyu *et al.*, "A method of using nonidentical resonant coils for frequency splitting elimination in wireless power transfer," *IEEE Trans. Power Electron.*, vol. 30, no. 11, pp. 6097–6107, Jul. 2015.

[20] W. Lee, H. L. Lee, K. Oh, and J. Yu, "Uniform magnetic field distribution of a spatially structured resonant coil for wireless power transfer," *Appl. Phys. Lett.*, vol. 100, Apr. 2012, Art. no. 214105.

[21] K. Lee, W. X. Zhong, and S. Y. R. Hui, "Effects of magnetic coupling of nonadjacent resonators on wireless power domino-resonator systems," *IEEE Trans. Power Electron.*, vol. 27, no. 4, pp. 1905–1916, Feb. 2012.

[22] N. Y. Kim, K. Y. Kim, and C. W. Kim, "Automated frequency tracking system for efficient mid-range magnetic resonance wireless power transfer," *Microw. Opt. Technol. Lett.*, vol. 54, pp. 1423–1426, Nov. 2012.

[23] T. C. Beh, M. Kato, T. Imura, S. Oh, and Y. Hori, "Automated impedance matching system for robust wireless power transfer via magnetic resonance coupling," *IEEE Trans. Ind. Electron.*, vol. 60, no. 9, pp. 3689–3698, Sep. 2013.

[24] J. Park, Y. Tak, Y. Kim, Y. Kim, and S. Nam, "Investigation of adaptive matching methods for near-field wireless power transfer," *IEEE Trans. Antennas Propag.*, vol. 59, no. 5, pp. 1769–1773, May 2011.

[25] W. S. Lee, W. I. Son, K. S. Oh, and J. W. Yu, "Contactless energy transfer systems using antiparallel resonant loops," *IEEE Trans. Ind. Electron.*, vol. 60, no. 1, pp. 350–359, Jan. 2013.

[26] W. Niu, J. Chu, W. Gu, and A. Shen, "Exact analysis of frequency splitting phenomena of contactless power transfer systems," *IEEE Trans. Circuits Syst. I, Reg. Papers*, vol. 60, no. 6, pp. 1670–1677, May 2013.

[27] Y. Li, Q. Yang and Z. Yan, "Analysis and validation on characteristic of orientation in wireless power transfer system via coupled magnetic resonances," *Trans. China Electrotech. Soc.*, vol. 29, pp. 197–203, Feb. 2014.

[28] Y. Li, Q. Yang and Z. Yan, "Characteristic of frequency in wireless via magnetic resonance coupling," *Elect. Mach. Control*, vol. 16, pp. 7–11, Jul. 2012.

[29] W. Q. Niu, W. Gu, J. X. Chu, and A. D. Shen, "Coupled-mode analysis of frequency splitting phenomena in CPT systems," *Electron. Lett.*, vol. 48, pp. 723–724, Jun. 2012.

[30] H. Nguyen and J. I. Agbinya, "Splitting frequency diversity in wireless power transmission," *IEEE Trans. Power Electron.*, vol. 30, no. 11, pp. 6088–6096, Jul. 2015.

[31] Z. Zhao, Y. Zhang, and K. Chen, "New progress of magnetically-coupled resonant wireless power transfer technology," in *Proc. CSEE*, Jan. 2013, vol. 33, pp. 1–13.

[32] Q. Yang, P. Zhang, and L. Zhu, "Key fundamental problems and technical bottlenecks of the wireless power transmission technology," *Trans. China Electrotech. Soc.*, vol. 5, pp. 1–8, May 2015.

[33] J. H. Fu and Z.-F. Fu, *Modal Analysis*. London, U.K.: Butterworth, 2001.

[34] K. Chen, *An Introduction to Mechanical Vibration*. Beijing, China: China Agricultural Univ. Press, 2014.

Yue Sun (M'07) received the B.E. degree in electrical engineering, the M.E. degree in industry automation, and the Ph.D. degree in mechanical electrical integrated manufacturing from Chongqing University, Chongqing, China, in 1982, 1988, and 1995, respectively.

In 1997, he was a Senior Visiting Scholar in France for one year. He is currently a Professor with the State Key Laboratory of Power Transmission Equipment & System Security and New Technology, and the College of Automation, Chongqing University. His research interests include automatic control, wireless power transfer, and power electronics applications.

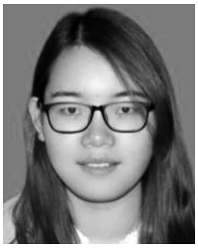

Zhi-Juan Liao received the B.E. degree in 2014 from the College of Automation, Chongqing University, Chongqing, China, where she is currently working toward the Ph.D degree in control theory and control engineering.

Her research interests include wireless power transfer and power electronics.

Zhao-Hong Ye received the B.E. and M.E. degrees in 2008 and 2011 from the College of Automation, Chongqing University, Chongqing, China, respectively, where he is currently working toward the Ph.D. degree in control theory and control engineering.

He is currently working as a Lecturer with the College of Automation, Chongqing University. His research interests include wireless power transfer, power electronics applications, and intelligent control.

Chun-Sen Tang (S'08–M'09) received the B.E. and Ph.D degrees from the College of Automation, Chongqing University, Chongqing, China, in 2004 and 2009, respectively.

In 2008, he was a Research Fellow with the Department of Electrical and Computer Engineering, The University of Auckland, Auckland, New Zealand. In 2009, he joined the College of Automation, Chongqing University, where he is currently an Associate Professor. His current research interests include nonlinear modeling and analysis, intelligent control, and wireless power transfer.

Pei-Yue Wang received the B.E. degree from the College of Mechanical and Electrical Engineering, Xidian University, Xi'an, China, in 2015. He is currently working toward the Ph.D. degree at the Control Theory and Control Engineering, College of Automation, Chongqing University, Chongqing, China.

His research interests include modeling and control of wireless power transfer and power electronics.